THE ROLE OF REGULARIZATION IN SHAPING WEIGHT AND NODE PRUNING DEPENDENCY AND DYNAMICS

Yael Ben-Guigui

The School of Electrical and Computer Engineering Ben-Gurion University Jacob Goldberger Engineering Faculty Bar-Ilan University Tammy Riklin-Raviv The School of Electrical and Computer Engineering Ben-Gurion University

ABSTRACT

The pressing need to reduce the capacity of deep neural networks has stimulated the development of network dilution methods and their analysis. While the ability of L_1 and L_0 regularization to encourage sparsity is often mentioned, L_2 regularization is seldom discussed in this context. We present a novel framework for **weight** pruning by sampling from a probability function that favors the zeroing of smaller weights. In addition, we examine the contribution of L_1 and L_2 regularization to the dynamics of **node** pruning while optimizing for **weight** pruning. We then demonstrate the effectiveness of the proposed stochastic framework when used together with a weight decay regularizer on popular classification models in removing 50% of the nodes in an MLP for MNIST classification, 60% of the filters in VGG-16 for CIFAR10 classification, and on medical image models in removing 60% of the channels in a U-Net for instance segmentation and 50% of the channels in CNN model for COVID-19 detection. For these node-pruned networks, we also present competitive weight pruning results that are only slightly less accurate than the original, dense networks.

1 Introduction

The advent of deeper and wider neural networks has made the need to reduce their storage and computational cost critical, especially for certain real-time applications. In particular, features such as model size, memory footprint, the number of floating point operations (FLOPs) and power usage which are directly related to the number of network parameters must be considered in resource-constrained setups such as mobile phones and wearable devices. In recent years there has been a significant effort to address the apparent trade-off between inference accuracy and reliability which requires sufficient network capacity and parameters' frugality, see [4] and references therein. However, having adequate network capacity and maintaining network compactness are not necessarily contradictory goals. It has been shown that neural networks are usually overparametrized and therefore can be pruned without hardly loss in accuracy [11, 38, 29]. Moreover, overparameterized neural networks can easily overfit and even memorize random patterns in the data [43], and thus lack the ability to generalize at inference time.

One straightforward approach to reducing the number of neural network' parameters consists of systematic weight or node pruning while training. In [12] the pruning phase was applied to parameters of an already trained and optimized neural network in an attempt to maintain similar accuracy. Most current methods follow this strategy since pruning from scratch was shown to be inferior [43, 26].

Since random pruning may reduce network accuracy [4], a pruning decision is usually based on some scoring criterion, e.g., absolute values or contributions to network activation or gradients. In this context it is worth noting that the optimal pruning criterion is debatable. In [17] it was suggested that a weight's magnitude is indicative of its usefulness in reducing the error, while other approaches have suggested more sophisticated "importance" criteria, and utilized the Hessian of the loss function [22, 14] or a Taylor expansion to approximate its changes due to pruning [30]. However, the latter approaches involve additional computational cost during training. The other main source of variability across different pruning algorithms are the timing and the way the pruning is carried out. Although setting thresholds below which nodes or edges are removed is useful [12] a stochastic approach that defines the probability for pruning is more elegant. However, some stochastic pruning algorithms involve thresholding as well, either because the weight zeroing is done temporarily - as in

Dropout based approaches [9, 29] or because the probabilistic gating mechanism is not binary [45]. Obviously, setting a threshold as well as the timing and frequency of its application requires determining the right balance between the pruning ratio and accuracy. All these hyperparameters are network-dependent and if the threshold is applied as part of a post-process, it cannot be learned during training.

A network can be pruned at different levels. While weight pruning is highly prevalent [11, 38, 29], node pruning, i.e., the removal of a node along with all of its in-going and out-going connections is considered to be more effective, reduces computational cost and is more suitable for hardware and software optimization [3, 41, 26, 31]. In the same manner, pruning can be applied to redundant channels [16] and kernels or filters [23, 28, 18, 15] to simplify convolutional neural networks or to directly reduce the FLOPS [1]. The level of pruning can be changed in any stage of the optimization, depending on the pruning objective [33]. However, to the best of our knowledge, simultaneous pruning of different levels with a single pruning objective has never been addressed. Moreover, most weight pruning algorithms achieve poor node pruning results, especially when weight pruning is done at the end of a training process based on some predefined criterion, e.g., the probability that all weights connected to a particular node will be zeroed is exponentially low.

In a recent line of works, regularization was employed to encourage sparsity. In [27] a differentiable approximation to L_0 regularization via the hard concrete distribution was used. Other methods have utilized the L_1 norm as an alternative approximation to L_0 , e.g., [25, 19]. However, while L_2 regularization is occasionally incorporated as part of a network's loss function [12, 11], its effect on the dynamics of the sparsity-constrained training process has not been examined.

The key contribution of the proposed study lies in utilizing weight decay regularization to facilitate pruning and understanding its role in manipulating pruning dynamics. Rather than using a fixed pruning criterion, we define a probability function and a gating mechanism such that weights with lower absolute values are more likely to be removed. Regularization then plays a triple role. Beyond its clear advantage in reducing overfitting, it decreases weight' values, thus increasing their pruning probability. Moreover, it turns out that while optimizing for weight pruning, node pruning is increased as well. Our experiments show that an application of a weight regularizer suppresses the tendency of edges to compensate for pruned edges that are connected to the same nodes.

The proposed method, dubbed Weight to Node Pruning (WtoNP), is applied to several standard network architectures, for both classification and segmentation and is compared to state-of-the-art weight and node pruning algorithms. Specifically we demonstrate its strength using a multilayer perceptron (MLP) and a VGG-16 for MNIST

and CIFAR-10 classification (respectively) and the U-Net for segmentation of cell microscopy data. The results show that our method is on a par with weight pruning algorithms and with node pruning algorithms. Moreover, the pruning of both weights and nodes has the clear advantage of reducing higher ratios of the parameters, thus saving storage space while more effectively reducing the computational cost. The code of the proposed pruning method, which can be easily adapted to neural networks of different architectures, will be made available upon the acceptance of this manuscript.

2 Stochastic weight pruning and regularization

Given a network architecture and a training dataset we aim to learn a sparse parameter set θ by optimizing a suitable objective function. Our explicit goal is weight pruning but we show that if a weight regularization function is added to the cost function, pruning of the network nodes also takes place. Our pruning method is based on zeroing each edge weight in a stochastic manner where the probability of a network parameter to be retained is proportional to its magnitude.

Let $h(\cdot,\theta)$ define a non-linear function parametrized by θ that represents a neural network. We define the network's loss function that includes the regularisation terms $L(\cdot)$ with respect to a given set of input-output pairs $\{x_i,y_i\}_{i=1}^n$ and a set of weights $\theta=(w_1,...,w_m)$ as follows:

$$L(\theta) = \frac{1}{n} \sum_{i=1}^{n} l(h(x_i; \theta), y_i) + \lambda \mathcal{R}(\theta)$$
 (1)

where $\mathcal{R}(\theta) = ||\theta||_p^p$ is the L_p norm regularization function of the weights, λ is a non-negative hyperparameter and $l(\cdot)$ corresponds to the model loss function. In [27] L_0 regularization was suggested to encourage weight sparsity. Here, in contrast, we focus on either L_1 or L_2 regularization. While the L_1 norm is often used as a differentiable approximation of L_0 , L_2 norm which encourages weight decay [13, 17] has not been used explicitly to encourage network sparsity. In the following, we show that once a stochastic weight gating function is applied that favors zeroing weights with smaller magnitudes, L_2 and L_1 regularizations are advantageous.

Recall that for L_2 , i.e., when $\mathcal{R}(\theta) \equiv ||\theta||_2^2 = \sum_{j=1}^m w_j^2$ the update step of a weight w_j by gradient decent optimizer is the following:

$$w_{i}^{t} = (1 - \lambda')w_{i}^{t-1} - \epsilon(\nabla_{w_{i}}l(\theta^{t-1}))$$
 (2)

where t counts the update steps, ϵ is the learning rate and $\lambda' = \lambda \epsilon$. Following [13, 17] we set $0 < \lambda' < 1$. When the gradient of $l(\theta)$ with respect to w_j is negligible, w_j shrinks in each step by a factor of $1 - \lambda'$.

Similarly, the update step in the presence of L_1 regularization is as follows:

$$w_i^t = w_i^{t-1} - \lambda' \operatorname{sign}(w_i^{t-1}) - \epsilon(\nabla_{w_i} l(\theta^{t-1}))$$
 (3)

which means that whether positive or negative, if $\nabla_{w_j} l(\theta^{t-1})$ is negligible, w_j is "pushed" to zero by λ' in each gradient descent step.

Our goal is to stochastically prune weights based on their magnitude, where weights with smaller magnitudes have a higher probability to be pruned. Each weight can be zero with a different probability, according to Bernoulli distribution ($\sim Bern(\cdot)$), depends on the weight magnitude. Therefore we use a function for mapping the weight magnitude to a probability. Let $\varphi:[0,\infty)\to[0,1]$ denote a monotonically increasing function and let z_j denote a binary gating variable $z_j\sim Bern\left(\varphi(|w_j|)\right)$. We propose a modified weight update during the parameter learning process as follows:

$$\tilde{w}_j^t = w_j^{t-1} - g\left(\nabla_{w_j}L(\theta^{t-1})\right) \qquad \quad j = 1,...,m \quad (4)$$

$$z_j^t \sim Bern\left(\varphi(|\tilde{w}_j^t|)\right)$$
 (5)

$$w_i^t = \tilde{w}_i^t \cdot z_i^t \tag{6}$$

where g() is an optimizer scheme. Several even functions can be considered to represent φ , e.g., a Gaussian shaped function $1 - \exp(-\frac{1}{2}aw^2)$, We can also use $1 - 4\sigma(aw)(1 - \sigma(aw))$ such that $\sigma()$ is the sigmoid function and a is a parameter that controls its slope.

The Weight to Node Pruning (WtoNP) is summarized in Algorithm 1 and the main concept is illustrated in figure 1. It is applied to a trained network performing an additional training session that enforces sparse solutions by stochastically selecting a set of weights to be dropped. The proposed strategy of random zeroing of network components resembles the Dropout algorithm [37]. The main difference is that dropout temporarily eliminates different fractions of the weights in each forward-backward session of a single instance and then restores the original weights' values. In our approach when a weight w is zeroed its previous value is discarded. In [9], on the other hand, the Dropout is applied to reduce model dependency on the unimportant edges, thereby potentially reducing the performance degradation as a result of post-processing pruning (via threshold application). In contrast, the proposed joint edge pruning and model optimization explicitly targets both the performance and the sparsity of the learned network. Louizos et al. use an adaptation of concrete dropout and Molchanov et al. [29] use variational dropout, both with trainable drop rates to the weights of the network. In these two works, in contrast to our method the number of trainable parameters was doubled.

In general, there is no direct connection between weight pruning and node pruning and there must be a different explicit loss function for each of the two pruning goals. In other words, weight pruning algorithms do not encourage other edges that enter the same node (a.k.a. neighbouring

```
Algorithm 1 Weight to Node Pruning (WtoNP) Algorithm
```

```
Training dataset: input-output pairs (\mathbf{x}, \mathbf{y}) \equiv \{x_i, y_i\}_{i=1}^n Parameters: Trainable network weights \theta = (w_1, ..., w_m) Trained neural network: h(\cdot, \theta) with respect to some loss function l(\mathbf{y}, h(\mathbf{x}, \theta)) and some optimizer scheme g(\cdot)
```

for each minibatch: do

```
Compute gradients with respect to the loss: L(\theta) = \frac{1}{n} \sum_{i=1}^{n} l(h(x_i;\theta), y_i) + \lambda \|\theta\|_p, \ p \in \{1,2\}. Update network parameters:  \begin{aligned} & \text{for } j = 1 \text{ to m do} \\ & w_j \leftarrow w_j - g\left(\nabla_{w_j} L(\theta)\right) \\ & \text{end for} \end{aligned}  Stochastically prune weights based on their magnitude:  \begin{aligned} & \text{for } j = 1 \text{ to m do} \\ & Z_j \sim Bern(\varphi(|w_j|)) \\ & \text{set } w_j \leftarrow w_j \cdot z_j \\ & \text{end for} \end{aligned}
```

edges) to be pruned together. In our scheme, a zeroed edge can move away from zero but since the updated weight is still small there is a good chance that it will be zeroed again and so on. In that case we can expect that the weights of the neighboring edges will become larger to compensate for the removed edge. However, if the network parameters are regularized, the rate of growth of edges that are neighbors of the zeroed edge is suppressed. This in turn causes the entire node to be less informative for the global network decision such that gradually the magnitudes of its edges will decrease as well until finally they will be zeroed. We demonstrate this dynamics for various network architectures in the experiment section.

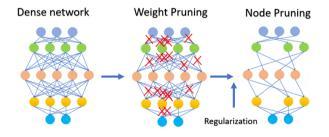


Figure 1: **Illustration of the WtoNP algorithm main concept.** The WtoNP algorithm is applied to a trained network by sampling weights and pruning them based on their magnitude. If a weight regularization function is added to the cost function, pruning of the network nodes also takes place.

3 Pruning performances, comparisons and analysis

To validate the effectiveness of our method, we applied it to two different classification tasks and instance segmentation. We employed several regularization terms: L_1 , L_2 and elastic-net, as well as no regularization. For all tasks, we initially reached a baseline model by training a full-size network until convergence. We then applied our pruning strategy to the trained network by performing a combined training and pruning session.

3.1 Implementation details

We tested the proposed pruning algorithm on four different network architectures performing four different tasks. The networks were trained using Adam optimizer [20] with the following (default) hyper-parameters: learning rate=0.001, β_1 =0.9 and β_2 =0.999. The only exception was the learning rate of the VGG-like network which was set to 0.0005. The proposed pruning technique is implemented as a K callback or fastai callback and therefore can easily incorporated in the training of any network regardles its architecture. We define the stochastic function ζ follows:

$$\varphi(w) = 1 - 4\sigma(aw)(1 - \sigma(aw)),$$

where σ denotes the standard sigmoid function. hyperparameter a which controls the slope of the sigmass tuned using the validation set. In our experiments a took values in the range of [1e-2, 1e-5].

MLP-300-100 for MNIST classification: The MLP-300-100 [22] is a fully connected network with two hidden layers, with 300 and 100 neurons each with 267K parameters. The baselines were trained for 200 epochs and the networks were diluted for another 200 epochs. We set $\lambda=1e-4$ for all regularizations terms in the pruning sessions.

VGG-like for CIFAR-10 classification: The VGG-like network was inspired by the original VGG-16 [36]. It is a standard convolution neural network with 13 convolutional layers followed by two fully connected layers with 512 and 10 neurons, respectively. The total number of trainable parameters is 15M. We used the CIFAR-10 dataset [21] to evaluate this model. The network was trained for 250 epochs with L2 regularization. For the pruning session we used $\lambda=5e-5$ and $\lambda=1e-5$ for L_2 and L_1 regularization, respectively.

U-Net for cell segmentation in microscopy images: The U-Net architecture which was initially introduced in [34] is a symmetrical fully convolutional network with skip connections, comprising a contracting path and an expansive path. The tested cell segmentation task and the dataset used are part of the ISBI 2012 segmentation challenge¹. For

this experiment we used the serial section Transmission Electron Microscopy (ssTEM) dataset of the Drosophila first instar larva ventral nerve cord (VNC) [2]. An example of a microscopy image from the tested dataset is presented in figure 2. To demonstrate the quality of the segmentation results, a manual segmentation (middle) of the cell image on the left is presented along with the U-Net prediction (right) after the pruning of 95% of its weights. The training data include 30 images (512 × 512 pixels) randomly partitioned into patches (128×128 pixels), where each training example is paired with a manual (ground truth) segmentation. For the test dataset which contains 30 images as well, evaluation was performed by the challenge organizers since the ground truth annotations were confidential. The U-Net was trained for 3000 epochs each session using cross entropy loss and data augmentation as in [34]. For the pruning sessions, we set the coefficient of all regularizations terms to $\lambda = 1e - 4$.

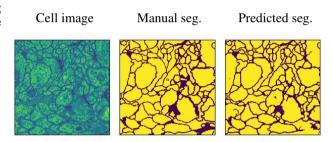


Figure 2: A microscopy image along with its segmentations. A cell microscopy image (left) along with its manual segmentation (middle) and its segmentation prediction by the U-Net following pruning of 95% of its weights.

DarkCovidNet Model for automatic COVID-19 detection using raw chest X-ray images: The DarkCovidNet architecture introduced in [32] and inspired by the DarkNet architecture. This model contains 17 convolution layers and uses for multi-class classification (COVID vs. No-Findings vs. Pneumonia). We used the dataset with which the model was trained in the original paper. This dataset contains 125 X-ray images diagnosed with COVID-19, 500 no-findings and 500 pneumonia class frontal chest X-ray images from two different sources [5, 40]. Figure 3 present example for chest X-ray images with COVID-19 case (left) Pneumonia case (middle) and No-Findings. 80% of the X-ray images are used for training and 20% for test. The model has been trained using the code published by [32] for 100 epochs. For the pruning sessions, we used $\lambda = 5e - 4$ and $\lambda = 1e - 4$ for L_2 and L_1 regularization, respectively.

3.2 Comparison of the different pruning techniques

We compared the WtoNP to the state-of-the-art weight and node pruning methods as shown in Table 1 and Table 2, respectively. The methods were evaluated based on their

¹http://brainiac2.mit.edu/isbi_challenge/

Table 1: Comparison to weight pruning algorithms

Model	Method	Error rate[%] ↓	% Pruned Weights ↑
MLP-300-100	LWC [12]	$1.64 \to 1.58$	91.77
(MNIST)	L-OBS [8]	$1.76 \to 1.82$	93.00
	Zhang et al [44]	$1.60 \to 1.60$	95.63
	SWS [38]	$1.89 \to 1.94$	95.70
	DNS [10]	$2.28 \to 1.99$	98.21
	GSM [7]	$1.81 \to 1.82$	98.34
	Autoprune [42]	$1.72 \to 1.78$	98.75
	WtoNP	$1.53 \to 1.71$	98.45
VGG-like	BLIND [35]	$6.75 \to 6.59$	86.10
(CIFAR-10)	Zhu et al [47]	$6.49 \to 6.69$	88.24
	Huang et al [18]	$7.23 \to 10.63$	92.80
	DCP [48]	$6.01 \to 5.43$	93.58
	SparseVD [29]	$7.55 \rightarrow 7.55$	98.46
	WtoNP	$6.46 \rightarrow 6.69$	93.86

Table 2: Comparison to node pruning methods

Model	Method	Error rate[%] ↓	% Pruned Nodes ↑	% Pruned Weights ↑
MLP-300-100	SparseVD [29]	$1.60 \to 1.80$	41.05	97.80
(MNIST)	BC [26]	$1.60 \to 1.80$	67.14	89.20
	L_0 [27]	$1.60 \to 1.80$	67.30	_
	NeST [6]	1.29	16.13*	97.05
	Autoprune [42]	$1.60 \to 1.82$	69.01	_
	WtoNP	$1.40 \to 1.73$	49.00	98.30
VGG-like	Li et al [23]	$6.75 \to 6.60$	37.12	64.00
(CIFAR-10)	StructuredBP [31]	$7.20 \to 7.50$	75.17	_
	Liu et al [24]	$7.53 \to 8.25$	47.35	36.00
	VCNN [45]	$6.75 \to 6.82$	62.00	73.34
	Wang et al [39]	6.87 o 6.85	59.10	91.80
	WtoNP	$6.46 \rightarrow 7.71$	60.34	83.53

Medical image networks pruned with WtoNP

Model	segmentation score (rand)↑		segmentation score (MI)↑		% Pruned Nodes ↑	% Pruned Weights ↑
U-Net	$96.37 \rightarrow 9$	06.43	$98.20 \to 98.22$		60.60	96.94
Model↑	precision ↑	recall^	f1-score↑	accuracy†	% Pruned Nodes↑	% Pruned Weights↑
DarkCovidNet	$89 \rightarrow 89$	$83 \rightarrow 82$	$85 \rightarrow 85$	$84 \rightarrow 85$	48	97

COVID-19



Pneumonia



No-Findings.



Figure 3: Chest X-ray images of COVID-19 case (left) Pneumonia case (middle) and No-Findings.

classification errors before and after the pruning procedure and the percentages of pruned weights or nodes. For MLP-300-100, we calculated the node percentage including the input layer, marking with * pruning methods that did not consider it. For the MLP-300-100 we obtained a weight pruning percentage of more than 98%, while maintaining higher accuracy than other pruning methods with similar pruning ratios. For the VGG comparison, 'pruned nodes'

Table 3: Pruning 90% of VGG-like weights on CIFAR-10

Regularization	Method	Zero node Ratio↑	Error rate[%]↓
L_2	WtoNP	26.9 ± 3.0	$\boldsymbol{9.0 \pm 0.2}$
	SKeras[46]	30.3 ± 5.8	10.4 ± 0.6
	TD[9]	0	9.6 ± 0.4
L_1	WtoNP	64.1 ± 2.3	9.8 ± 0.1
	SKeras[46]	53.0 ± 8.9	8.3 ± 0.6
	TD [9]	0	10.0 ± 0.2
without	WtoNP	$\boldsymbol{1.7 \pm 0.5}$	8.2 ± 0.3
	SKeras[46]	0.1 ± 0.1	17.7 ± 0.8
	TD [9]	0	10.5 ± 0.3

indicate the kernels' prune percentage. Note the relatively low error rate (6.69) with the high percentage of weight pruning (93.86%) that was obtained using our WtoNP. In addition, our method presented competitive nodes pruning performances, by pruning 60% of the VGG network kernels. Pruning results of networks for medical application

are barely reported in the literature. Bear in mind that though less than 4% of the U-Net weights remained, the segmentation scores were improved. For the DarkCovidNet Model we obtained 97% weight pruning similar classification reports, with higher accuracy and minor drop on the recall. The results reported in Tables 1-2 were obtained using L_2 regularization.

We next tested the impact of L_1 and L_2 regularizations on pruning performance for the VGG-like network using the WtoNP and two other pruning approaches that originally did not include a regularization term. Specifically, we used a standard Keras implementation of magnitude-based weight pruning [46] and an implementation of the targeted Dropout algorithm [9] with a TensorFlow backend 2 . Table 3 presents the comparisons for pruning 90% of the weights. It shows that the presence of a regularization term facilitated node pruning for the magnitude-based weight pruning method in [46] as well. On the other hand, regularization did not influence the targeted Dropout pruning method since the pruning in that case is done as a post-processing step.

3.3 Analysis of pruning structure for different regularizations

In this section, we presents further pruning results obtained using L_1, L_2 and elastic net regularizations for the VGG, MLP, U-Net and DaekCovidNet networks and investigate the pruning structure in particular layers for the MLP-300-100 and the U-Net architectures.

Table 4 presents further pruning results obtained using L_1, L_2 and the elastic-net regularizations with respect to no regularization at all for the different neural network architectures. For fair comparison, in all experiments we kept the percentage of pruned weights fixed and present the respective accuracy and percentage of pruned nodes. As expected, there is a trade-off between these measures, where L_1 is preferable for the VGG-like network when the main objective is to maximize the percentage of pruned nodes, whereas L_2 works the best in all respects for the U-Net. We stress that in all experiments the pruning process was applied directly to the weights and not to the nodes (kernels), while tuning λ and a to achieve the desired percentage of pruned weights.

MLP-300-100 for MNIST classification: The MLP-300-100 is composed of an input layer with 784 nodes, two fully connected hidden layers, termed FC1 and FC2 containing 300 and 100 nodes, respectively, and an output layer with 10 nodes, where each node represents a digit. Figure 4 presents a visualization of the weights of the edges connecting between the consecutive MLP layers. The first row in the figure presents binary maps of the remaining connections between the input layer (784 nodes) and the first hidden layer (300 nodes) after pruning with either the L_1 (left) or L_2 (middle) regularization terms or without

any regularization (right). While the number of removed connections (black) seems to be similar in all the plots, the patterns of the remaining connections for the regularized pruning appear to be much more coherent, which means that entire rows and columns (nodes) were removed. On the other hand, when no regularization was applied, the pattern of remaining connections was random. The second row presents the weights (color coded) of the edges connecting the second hidden layer (100 nodes) to the output layer (10 nodes) visually. Note that for the regularized pruning, very few nodes were required to represent each of the output digits. In addition, as expected, the magnitudes of the remaining connections for the pruning with L_2 regularization were much lower. The weights' color map for unregularized pruning was much denser, with many more active nodes (columns) in general. Note however (see also first row in table 5 and figure 5) that the average number of nodes require to represent each digit is similar to one obtained using pruning with L_2 regularization. The maps presented in the figure correspond to the results shown in Table 4 when pruning 97% of the weights.

In the next experiment we examined the average number of nodes required to represent an MNIST digit. Note that in the original unpruned network, most of the 100 nodes in FC2 were connected to all 10 nodes in the output layer, where each node represents a single digit. Figure 5 and Table 5 present the average number of nodes in FC2 that remained connected to each of the nodes in the output layer for different regularization schemes. These average numbers are presented for the case of 95% pruned weights (Table 5) and as a function of the percentage of pruned weights (Figure 5). The last row in Table 5 presents the percentages of pruned nodes in FC2 when 95% of the pruned weights were removed. Note that we ran each experiment 4 to 6 times so that the tables include standard deviation values, shown as error-bars in the figures.

U-Net for cell segmentation in microscopy images: Figure 6 presents the U-Net architecture (lower panel) along with the respective bar plot (upper panel) listing the percentages of pruned kernels in each layer. Recall that the U-Net was diluted by direct pruning of its weights. In the presence of L_1 (blue), L_2 (red) and elastic-net (yellow) regularizations throughout the weight pruning process, complete U-Net's kernels were pruned as well. As expected, the node pruning percentages were much lower when no regularization was applied (purple bars). Table 6 presents the respective percentages of pruned weights and kernels in the entire network along with the segmentation scores for the test data.

DarkCovidNet Model for automatic COVID-19 detection using raw chest X-ray images:

Figure 7 presents the DarkCovidNet architecture (lower panel) along with the respective bar plot (upper panel) listing the percentages of pruned kernels in each layer for weights pruning percentage of 97%. In the presence of L_1 (blue), L_2 (red) regularizations throughout the weight

²https://pypi.org/project/keras-targeted-dropout/

Table 4: Pruning Results for Different Regularizations

Model	Reg	Top-1 Error[%]	% Pruned nodes	% Pruned weights
MLP-300-100	L_1	2.57 ± 0.2	42.30 ± 0.8	92
	L_2	1.66 ± 0.1	34.80 ± 0.7	
	Elastic-net	2.28 ± 0.2	41.40 ± 0.7	
	No-regularization	1.71 ± 0.1	13.30 ± 0.4	
	L_1	2.28 ± 0.1	45.90 ± 0.7	97
	L_2	1.76 ± 0.1	47.40 ± 0.7	
	Elastic-net	1.98 ± 0.1	45.80 ± 0.7	
	No-regularization	2.18 ± 0.3	16.07 ± 2.2	
VGG-like	L_1	9.79 ± 0.1	64.07 ± 2.3	90
	L_2	8.97 ± 0.2	26.96 ± 3.1	
	No-regularization	8.17 ± 0.3	1.68 ± 0.5	
	L_1	10.10 ± 0.2	69.86 ± 1.0	95
	L_2	8.86 ± 0.2	17.10 ± 4.3	
	No-regularization	8.29 ± 0.2	1.86 ± 0.3	

Model	Reg	seg score (rand)↑		segm score (MI)		% Pruned Nodes	% Pruned Weights
U-Net	L_1	94.48 ± 0.7		97.43 ± 0.1		1.45 ± 0.2	95
	L_2	95.81 ± 0.7		98.12 ± 0.2		68.05 ± 5.9	
	Elastic-net	94.25 ± 0.6		97.39 ± 0.7		3.46 ± 2.5	
	No-regularization	94.28 ± 0.8		97.72 ± 0.1		0	
Model↑	Reg	precision ↑	recall†	f1-score↑	accuracy†	% Pruned Nodes↑	% Pruned Weights↑
DarkCovidNet	L_1	88.67 ± 0.4	82.33 ± 1.4	84.50 ± 0.7	84.00 ± 0.1	68.87 ± 0.6	97
	L_2	88.28 ± 0.5	81.72 ± 1.3	84.17 ± 0.9	84.00 ± 0.7	40.07 ± 8.4	
	No-regularization	88.89 ± 1.6	83.00 ± 1.4	85.11 ± 1.1	84.33 ± 2.0	0 ± 0	

Table 5: The average number of nodes in FC2 that remained connected to a node in the output layer (nodes per digits) and the percentage of pruned nodes in FC2 for MLP-300-100 with different regularization schemes. ↓ lower is sparser, ↑ higher is sparser.

Regularization	# nodes per digit	% pruned nodes in FC2
L_1	11.8 ± 1.0	84.7 ± 1.4
L_2	24.4 ± 2.7	64.8 ± 3.1
elastic-net	11.8 ± 0.9	80.4 ± 1.9
w/o reg.	21.7 ± 1.5	3.5 ± 2.1

Table 6: Percentages of the pruned kernels and weights in the entire network along with the segmentation (seg.) scores in the presence of L_1 , L_2 , or elastic-net regularization terms or without any regularization.

, _C					
	L_1	L_2	Elastic-net	w/o reg	
% pruned kernels	75.4	82.0	82.3	36.5	
% pruned weights	99.9	99.7	99.8	99.8	
seg. score (MI)	97.6	97.7	97.3	97.5	
seg. score (Rand)	94.9	95.1	93.9	95.0	

pruning process, complete kernels of the deeper layers were pruned. This indicates that there is redundancy, especially in the deep layers. When no regularization was applied, the node pruning percentage is zero.

Table 7: Node and weight pruning percentages in MLP-300-100 when L_2 regularization was applied for different values of λ . The results refer to Figure 8 in the main paper.

	2e-4	6e - 4	12e - 4
% pruned weights	97.7 ± 0.1	98.5 ± 0.1	98.9 ± 0.1
% pruned nodes	48.2 ± 1.1	53.9 ± 0.7	57.7 ± 0.9

4 Analysis of pruning dynamics

In this section, we investigate the influence of different regularization terms on the dynamics and the structure of weight and node pruning for different network architectures. To highlight the robustness of the pruning dynamics we ran each of the experiments 4 to 6 times for different sets of initial weights. Specifically, we initialized the first training sessions (prior to the pruning) using different sets of random weights. As a result, the initial weights of the pruning sessions were different for each run. The plots are therefore shown with error bars.

Regularization strength: In Figure 8 we present the dynamics of weight and node pruning for the MLP-300-100 using three different values of L_2 regularization coefficients λ . As expected, the percentage of **pruned weights** increased as λ took on higher value since the regularization was stronger. However, the change in the percentage of **pruned nodes** as a function of λ was higher. Table 7 presents the final pruning results.

Regularization terms: In the next experiment we compared the effects of L_1 , L_2 and elastic-net regularizations

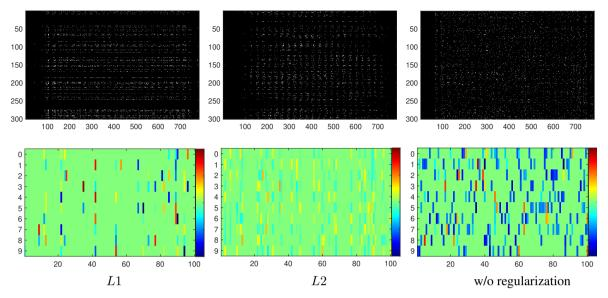


Figure 4: Visualization of the remaining connections between consecutive layers in MLP-300-1000 after pruning with L_1 and L_2 (left, middle) and without (right) regularization. The first row in the figure presents binary maps of the remaining connections between the input layer (784 nodes) and the first hidden layer (300 nodes). The second row is a visual presentation of the weights (color coded) of the edges connecting the second hidden layer (100 nodes) to the output layer (10 nodes).

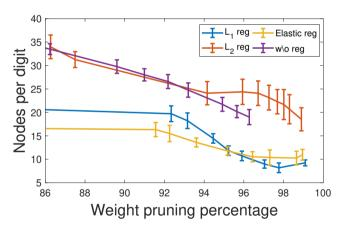


Figure 5: The average number of nodes representing an MNIST digit as a function of the weight pruning percentage for MLP-300-100. Results are shown for pruning with L_1 , L_2 and elastic-net as well as without regularization.

with respect to training with no regularization - on the dynamics of weight and node pruning for four different architectures. The plots presented in Figure 9 shows the weight/node pruning percentages as a function of the number of epochs. In the absence of a regularization term (purple plots) node pruning percentage was either low (MLP) or negligible (VGG, U-Net, DarkCovidNet) whereas weight pruning percentage was relatively high.

The plots presented for the MLP-300-100 show that L_1 (blue), L_2 (red) and the elastic-net (yellow) regularization terms had similar influence on node and weight pruning dynamic and percentages. Different patterns of node pruning dynamics of the VGG and the U-Net architectures were observed for the different regularization terms. It appeared that L_1 regularization was preferable for VGG node pruning, yet for weight pruning L_2 was preferable. Overall using L_2 regularization for U-Net provided better segmentation performances, yet better node and weight pruning ratios were obtained by either L_1 or elastic-net regularizations.

Weight compensation and weight decay: Finally, we tested our hypothesis that when no regularization is applied, the magnitudes of edges that are neighbors of zero edges (connected to the same nodes) increase to compensate for the missing edges while in the presence of a regularization term, this compensation mechanism is suppressed and gradually entire nodes are zeroed. The results of this experiment are presented in Figure 10. To assess our assumptions, we chose a specific layer for each of the four architectures. We then calculated, for each epoch, the mean ratio of pruned weights per node (magenta) and the mean magnitude of non-zero weights per node (blue). The size of the error bars presents the average variance per node. The first row in Figure 10 presents the results obtained without regularization. Since a very high percentage of the weights were pruned, the mean ratio of pruned weights per node (magenta plot) almost reached one. Yet, the nodes themselves were not zeroed as the magnitudes of

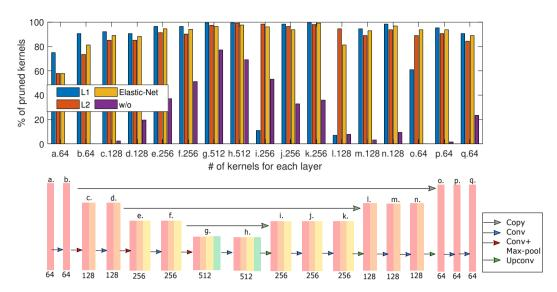


Figure 6: The U-Net architecture along with its respective bar plot presenting the percentage of pruned kernels in each of its layers. Lower panel: visualization of the U-Net architecture. The U-Net is composed of convolutional encoder layers of decreasing size followed by convolutional decoder layers of increasing size. In addition, corresponding encoder-decoder layers are connected with skip connections. The number of kernels in each layer is indicated underneath the bar that represents it.

Upper panel: percentage of pruned kernels in each layer for the U-Net architecture for L_1 , L_2 , elastic-net regularization and no regularization. (top image).

Modifies U-net architecture were each box corresponds to a multi-channel feature map, with the number of channels indicated below the box. Arrows in different colors denote different operations. The gray arrows correspond to copied feature maps. (bottom image).

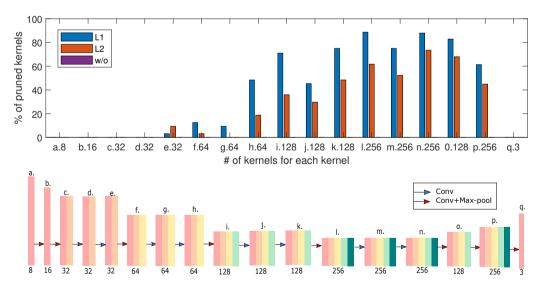


Figure 7: The DarkCovidNet architecture along with its respective bar plot presenting the percentage of pruned kernels in each of its layers. Lower panel: visualization of the DarkCovidNet architecture. TheDarkCovidNet is composed of convolutional layers of decreasing size. The number of kernels in each layer is indicated underneath the bar that represents it.

Upper panel: percentage of pruned kernels in each layer for the DarkCovidNet architecture for L_1 , L_2 and no regularization. (top image).

DarkCovidNet architecture were each box corresponds to a multi-channel feature map, with the number of channels indicated below the box. Arrows in different colors denote different operations. (bottom image).

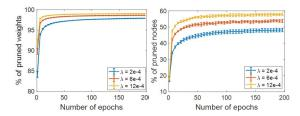


Figure 8: Pruning dynamics for MLP-300-100 applied to the MNIST classification. Weight (left) and node (right) pruning percentages as a function of the number of epochs. Three sets of experiments were conducted using L_2 regularization with different values $\lambda = 2e-4, 6e-4, 12e-4$ in blue, red and yellow, respectively.

the remaining weights gradually increased to compensate for the missing weights. The second and the third rows of Figure 10 present pruning dynamic results when L_2 regularization is applied. The plots in the second row present the results for nodes that were not zeroed throughout the entire pruning process. Similar to the experiments with no regularization (first row) the magnitudes of the remaining weights in the none-zero nodes increased to compensate for the zeroed weights. However, the increment in the mean magnitude was much larger and the variance in magnitude was higher, probably to compensate for the large number of zeroed nodes. The plots in the third row of Figure 10 present the mean results for nodes that eventually decreased to zero. For these nodes the regularization suppressed the tendency of the non-zero weights to grow in order to compensate for their neighboring zeroed weights. Eventually, these weights were also zeroed, as shown in the blue plots. Note that the corresponding average ratio of pruned weights per nodes (magenta) increased to 1.

5 Conclusions

We presented a general stochastic approach for neural network pruning which is indifferent to the network architecture, its training regime and its loss function. The method is shown to be effective for concurrent weight and node pruning. This is accomplished by utilizing weight decay regularization to facilitate pruning and understanding its role in manipulating pruning dynamics. Rather than using a fixed pruning criterion, we defined a probability function and a gating mechanism such that weights with lower absolute values were more likely to be removed. Regularization then played a triple role. Beyond its clear advantage in reducing overfitting, it decreased the weights magnitudes thus increasing their pruning probability. Moreover, while optimizing for weight pruning, node pruning was increased as well. We empirically studied the mechanism for this effect. Specifically, we showed that the L_1 and L_2 regularization term suppressed the 'tendency' of non-zero weights to compensate for neighboring pruned edges associated with the same nodes. Finally, we showed that the pruning results were on a par with both best the weight and node pruning algorithms for different widely used image classification and segmentation architectures.

References

- [1] Aflalo, Y., Noy, A., Lin, M., Friedman, I., Zelnik, L., 2020. Knapsack pruning with inner distillation. arXiv preprint arXiv:2002.08258.
- [2] Arganda-Carreras, I., Turaga, S.C., Berger, D.R., Cireşan, D., Giusti, A., Gambardella, L.M., Schmidhuber, J., Laptev, D., Dwivedi, S., Buhmann, J.M., et al., 2015. Crowdsourcing the creation of image segmentation algorithms for connectomics. Frontiers in neuroanatomy 9, 142.
- [3] Augasta, M.G., Kathirvalavakumar, T., 2013. Pruning algorithms of neural networks—a comparative study. Central European Journal of Computer Science 3, 105–115.
- [4] Blalock, D., Ortiz, J.J.G., Frankle, J., Guttag, J., 2020. What is the state of neural network pruning? arXiv preprint arXiv:2003.03033.
- [5] Cohen, J.P., Morrison, P., Dao, L., 2020. Covid-19 image data collection. arXiv 2003.11597 URL: https://github.com/ieee8023/ covid-chestxray-dataset.
- [6] Dai, X., Yin, H., Jha, N.K., 2019. Nest: A neural network synthesis tool based on a grow-and-prune paradigm. IEEE Transactions on Computers 68, 1487–1497.
- [7] Ding, X., Zhou, X., Guo, Y., Han, J., Liu, J., et al., 2019. Global sparse momentum sgd for pruning very deep neural networks, in: Advances in Neural Information Processing Systems, pp. 6379–6391.
- [8] Dong, X., Chen, S., Pan, S., 2017. Learning to prune deep neural networks via layer-wise optimal brain surgeon, in: Advances in Neural Information Processing Systems, pp. 4857–4867.
- [9] Gomez, A.N., Zhang, I., Swersky, K., Gal, Y., Hinton, G.E., 2019. Learning sparse networks using targeted dropout. arXiv preprint arXiv:1905.13678.
- [10] Guo, Y., Yao, A., Chen, Y., 2016. Dynamic network surgery for efficient dnns, in: Advances in neural information processing systems, pp. 1379–1387.
- [11] Han, S., Mao, H., Dally, W.J., 2015a. Deep compression: Compressing deep neural networks with pruning, trained quantization and huffman coding. arXiv preprint arXiv:1510.00149.
- [12] Han, S., Pool, J., Tran, J., Dally, W., 2015b. Learning both weights and connections for efficient neural network, in: Advances in neural information processing systems, pp. 1135–1143.

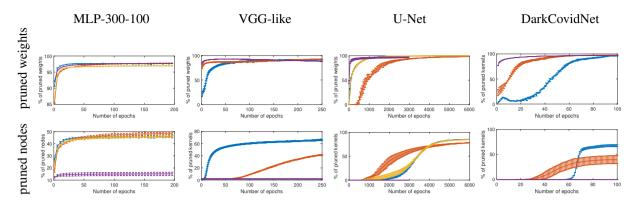


Figure 9: Percentages of pruned weights (left) and pruned kernels/nodes (right) for MLP-300-100 (first row), for VGG-like (second row), the U-Net (third row) and DarkCovidNet (forth row) calculated for each epoch. The plots are presented for different regularization terms: L_1 (blue), L_2 (red) and elastic-net (yellow) and with no regularization (purple).

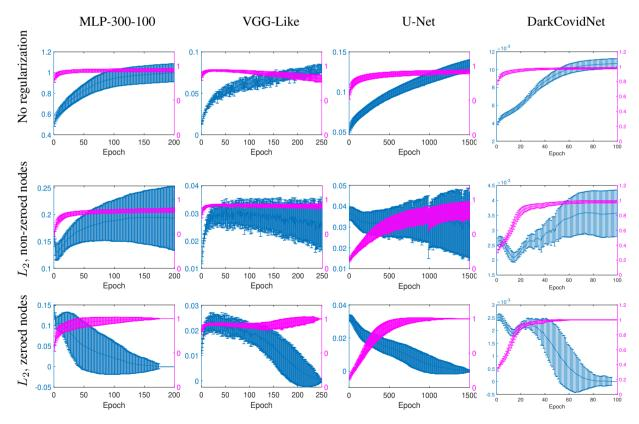


Figure 10: The mean value of non-zero weights per node (blue) and the mean ratio of pruned weights per node (magenta) for each epoch. The first row displays pruning dynamics w/o regularization, the second and third rows display pruning dynamics with L2 regularization of the non-zeroed nodes (second) and the zeroed nodes (third).

- [13] Hanson, S.J., Pratt, L.Y., 1989. Comparing biases for minimal network construction with backpropagation, in: Advances in neural information processing systems, pp. 177–185.
- [14] Hassibi, B., Stork, D.G., 1993. Second order derivatives for network pruning: Optimal brain surgeon, in: Advances in neural information processing systems, pp. 164–171.
- [15] He, Y., Liu, P., Wang, Z., Hu, Z., Yang, Y., 2019. Filter pruning via geometric median for deep convolutional neural networks acceleration, in: Proceedings of the IEEE Conference on Computer Vision and Pattern Recognition, pp. 4340–4349.
- [16] He, Y., Zhang, X., Sun, J., 2017. Channel pruning for accelerating very deep neural networks, in: Proceedings of the IEEE International Conference on Computer Vision, pp. 1389–1397.
- [17] Hinton, G.E., et al., 1986. Learning distributed representations of concepts, in: Proceedings of the eighth annual conference of the cognitive science society, p. 12.
- [18] Huang, Q., Zhou, K., You, S., Neumann, U., 2018. Learning to prune filters in convolutional neural networks, in: IEEE Winter Conference on Applications of Computer Vision (WACV), pp. 709–718.
- [19] Huang, Z., Wang, N., 2018. Data-driven sparse structure selection for deep neural networks, in: Proceedings of the European conference on computer vision (ECCV), pp. 304–320.
- [20] Kingma, D.P., Ba, J., 2014. Adam: A method for stochastic optimization. arXiv preprint arXiv:1412.6980.
- [21] Krizhevsky, A., Hinton, G., et al., 2009. Learning multiple layers of features from tiny images .
- [22] LeCun, Y., Denker, J.S., Solla, S.A., 1990. Optimal brain damage, in: Advances in neural information processing systems, pp. 598–605.
- [23] Li, H., Kadav, A., Durdanovic, I., Samet, H., Graf, H.P., 2016. Pruning filters for efficient convnets. arXiv preprint arXiv:1608.08710.
- [24] Liu, C., Wu, H., 2019. Channel pruning based on mean gradient for accelerating convolutional neural networks. Signal Processing 156, 84–91.
- [25] Liu, Z., Li, J., Shen, Z., Huang, G., Yan, S., Zhang, C., 2017. Learning efficient convolutional networks through network slimming, in: Proceedings of the IEEE International Conference on Computer Vision, pp. 2736–2744.
- [26] Louizos, C., Ullrich, K., Welling, M., 2017a. Bayesian compression for deep learning, in: Advances in Neural Information Processing Systems, pp. 3288–3298.

- [27] Louizos, C., Welling, M., Kingma, D.P., 2017b. Learning sparse neural networks through $l_{-}0$ regularization. arXiv preprint arXiv:1712.01312.
- [28] Luo, J.H., Wu, J., Lin, W., 2017. Thinet: A filter level pruning method for deep neural network compression, in: Proceedings of the IEEE international conference on computer vision, pp. 5058–5066.
- [29] Molchanov, D., Ashukha, A., Vetrov, D., 2017. Variational dropout sparsifies deep neural networks, in: Proceedings of the International Conference on Machine Learning, pp. 2498–2507.
- [30] Molchanov, P., Tyree, S., Karras, T., Aila, T., Kautz, J., 2016. Pruning convolutional neural networks for resource efficient transfer learning. arXiv preprint arXiv:1611.06440 3.
- [31] Neklyudov, K., Molchanov, D., Ashukha, A., Vetrov, D.P., 2017. Structured bayesian pruning via lognormal multiplicative noise, in: Advances in Neural Information Processing Systems, pp. 6775–6784.
- [32] Ozturk, T., Talo, M., Yildirim, E.A., Baloglu, U.B., Yildirim, O., Acharya, U.R., 2020. Automated detection of covid-19 cases using deep neural networks with x-ray images. Computers in Biology and Medicine, 103792.
- [33] Pasandi, M.M., Hajabdollahi, M., Karimi, N., Samavi, S., 2020. Modeling of pruning techniques for deep neural networks simplification. arXiv preprint arXiv:2001.04062.
- [34] Ronneberger, O., Fischer, P., Brox, T., 2015. U-net: Convolutional networks for biomedical image segmentation, in: International Conference on Medical image computing and computer-assisted intervention, Springer. pp. 234–241.
- [35] Salama, A., Ostapenko, O., Klein, T., Nabi, M., 2019. Prune your neurons blindly: Neural network compression through structured class-blind pruning, in: IEEE International Conference on Acoustics, Speech and Signal Processing (ICASSP), pp. 2802–2806.
- [36] Simonyan, K., Zisserman, A., 2014. Very deep convolutional networks for large-scale image recognition. arXiv preprint arXiv:1409.1556.
- [37] Srivastava, N., Hinton, G., Krizhevsky, A., Sutskever, I., Salakhutdinov, R., 2014. Dropout: a simple way to prevent neural networks from overfitting. The journal of machine learning research 15, 1929–1958.
- [38] Ullrich, K., Meeds, E., Welling, M., 2017. Soft weight-sharing for neural network compression. arXiv preprint arXiv:1702.04008.
- [39] Wang, W., Zhu, L., Guo, B., 2019. Reliable identification of redundant kernels for convolutional neural network compression. Journal of Visual Communication and Image Representation 63, 102582.
- [40] Wang, X., Peng, Y., Lu, L., Lu, Z., Bagheri, M., Summers, R., 2017. Hospital-scale chest x-ray database

- and benchmarks on weakly-supervised classification and localization of common thorax diseases, in: IEEE CVPR.
- [41] Wen, W., Wu, C., Wang, Y., Chen, Y., Li, H., 2016. Learning structured sparsity in deep neural networks, in: Advances in neural information processing systems, pp. 2074–2082.
- [42] Xiao, X., Wang, Z., Rajasekaran, S., 2019. Autoprune: Automatic network pruning by regularizing auxiliary parameters, in: Advances in Neural Information Processing Systems, pp. 13681–13691.
- [43] Zhang, C., Bengio, S., Hardt, M., Recht, B., Vinyals, O., 2016. Understanding deep learning requires rethinking generalization. arXiv preprint arXiv:1611.03530.
- [44] Zhang, T., Ye, S., Zhang, K., Tang, J., Wen, W., Fardad, M., Wang, Y., 2018. A systematic dnn weight pruning framework using alternating direction method of multipliers, in: Proceedings of the European Conference on Computer Vision (ECCV), pp. 184–199.
- [45] Zhao, C., Ni, B., Zhang, J., Zhao, Q., Zhang, W., Tian, Q., 2019. Variational convolutional neural network pruning, in: Proceedings of the IEEE Conference on Computer Vision and Pattern Recognition, pp. 2780–2789.
- [46] Zhu, M., Gupta, S., 2017. To prune, or not to prune: exploring the efficacy of pruning for model compression. arXiv preprint arXiv:1710.01878.
- [47] Zhu, X., Zhou, W., Li, H., 2018. Improving deep neural network sparsity through decorrelation regularization., in: International Joint Conferences on Artificial Intelligence, pp. 3264–3270.
- [48] Zhuang, Z., Tan, M., Zhuang, B., Liu, J., Guo, Y., Wu, Q., Huang, J., Zhu, J., 2018. Discriminationaware channel pruning for deep neural networks, in: Advances in Neural Information Processing Systems, pp. 875–886.